Surface Menshutkin S_N2 Reaction on Basic Gold Clusters Provides Novel Opportunities for the Cationization and Functionalization of Molecular Metal Clusters

Kunihiro Narita[a], Yohei Ishida[a,*], Shuichi Nukui[a], Zhong Huang[a,b], and Tetsu Yonezawa[a,*]

[a]Division of Material Science and Engineering, Faculty of Engineering, Hokkaido University, Kita 13 Nishi 8, Kita-ku, Sapporo, Hokkaido 060-8628, Japan.

[b]The State Key Laboratory of Refractories and Metallurgy, Wuhan University of Science and Technology, No. 947 Heping Rd, Wuhan 430081, China.

ABSTRACT

Surface chemical reactions on atomically precise metal clusters have considerable attention for opening a new platform for cluster functionalization. In this study, basic Au_{25}(4-PyET)$_{18}$ (4-PyET = –SCH_2CH_2Py; Py = pyridyl) clusters were successfully transformed into cationized Au_{25}(4-PyET-CH_3^+)$_x$(4-PyET)$_{18-x}$ clusters, without altering their Au_{25} cores, through the Menshutkin S_N2 reaction of their surface Py moieties. This study offers not only a simple cationization method, but also a protocol for modifying the surface functionalities of molecular metal clusters via a synthetic reaction.

TOC Graphic

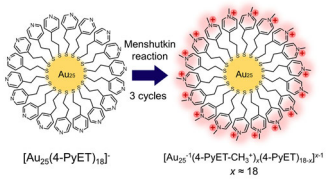

Atomically precise, thiolate-protected gold clusters ($Au_m(SR)_n$) have potential applications in diverse fields, such as catalysis,[1,2] sensing,[3,4] and bio-applications,[5,6] owing to their interesting physicochemical properties. Surface SR ligands are of particular interest as they affect the magic size (stable number of metal atoms) and structures of the clusters.[6,7] Furthermore, the R-groups on the cluster surface are exposed to solutions and other phases; hence, they determine the molecular-like characteristics of clusters,[8] such as their hydrophobicities/hydrophilicities,[9] chiralities,[10] catalytic activities,[2,11] optical properties,[12] and interactions with host materials.[5,6] These R-groups are therefore crucial to the rational design

of the functional properties and applications of clusters. In peculiar, clusters capped by cationic R-groups are desirable as they widen the applications of bioimaging and sensing;[13] however, the synthesis of cationized clusters is rarely reported owing to the difficulty in handling the positive charges of R-groups.[14-16] By preventing the formation of $[Au(I)]^-$–SR^+ ionic polymer complexes that hinder the homogeneous reduction of Au precursors and the formation of atomically pure clusters, we recently succeeded in the synthesis of cationized Au clusters ($Au_{25}(S(CH_2)_{11}N(CH_3)_3^+)_{18}$,[14] $Au_{144}(S(CH_2)_{11}N(CH_3)_3^+)_{60}$,[15] and $Au_{25}(S(CH_2)_{11}N(CH_3)_3^+)_x(S(CH_2)_2Ph)_{18-x}$ (x=1-6)).[16]

To date, major protocols for the preparation of atomically precise clusters with various thiolate ligands have been categorized into size-focusing[14,15] and ligand-exchange method.[16,17] In the former case, the Au(I)–SR complex is prepared by mixing Au ion and thiols (HSR), followed by reduction into objected Au clusters. The latter involves the synthesis of Au clusters, followed by the replacement of their initial ligands with the desired ligands. Besides these methods, surface reactions have also received significant attention in recent years; however, there are few reports on such reactions, two of which are azido- and amide-bond formation reactions.[18,19]

The Menshutkin S_N2 reaction is a common method to obtain quaternary ammonium salt ($[–N(CH_3)_3]^+$) by reacting a tertiary amine with an alkylating agent.[20] In this study, we demonstrate the Menshutkin (methylation) reaction of the surface pyridyl (Py) moieties on basic $Au_{25}(4\text{-PyET})_{18}$ clusters (4-PyET = $–SCH_2CH_2Py$) for their successful transformation into cationized $Au_{25}(4\text{-PyET-}CH_3^+)_x(4\text{-PyET})_{18-x}$ ($x \approx 18$) clusters (Scheme 1). This work proposes a novel strategy for not only the cationization of Au clusters by surface chemical reactions, but their functionalization as well.

Scheme 1. Menshutkin (methylation) reaction on $Au_{25}(4\text{-PyET})_{18}$ clusters. 4-PyET = $–SCH_2CH_2Py$, where Py = pyridyl group.

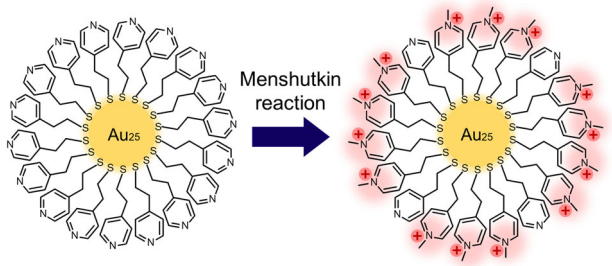

$[Au_{25}(4\text{-PyET})_{18}]^-$ $[Au_{25}^{-1}(4\text{-PyET-}CH_3^+)_x(4\text{-PyET})_{18-x}]^{x-1}$

The following 4 chemicals were evaluated as methylating reagents: iodomethane (MeI), dimethyl sulfate (Me_2SO_4), methyl trifluoromethanesulfonate (TfOMe), and trimethyl

oxonium tetrafluoroborate (Me_3OBF_4) (reactivity with Py group: MeI < Me_2SO_4 < TfOMe < Me_3OBF_4). The surface-reactive basic Au cluster $Au_{25}(4\text{-PyET})_{18}$ was synthesized according to our method as reported previously and characterized by electrospray ionization mass spectrometry (ESI-MS) and UV-vis absorption (Figure S1).[21] Figures 1(a)-(d) show the UV-vis absorption spectra of the samples before (0 min) and after the methylation reaction (30 min or 60 min) using each of the 4 methylating reagents. When MeI and Me_3OBF_4 were used (Figures 1(a) and (d), respectively), the characteristic absorption peaks of Au_{25} clusters[22,23] at 400, 450, 560, 670 and 780 nm disappeared after the reaction, indicating that these reagents decomposed the Au_{25} clusters. On the other hand, no obvious decreases in the absorption spectra were observed when using Me_2SO_4 and TfOMe (Figures 1(b) and (c)). The decomposition of the clusters by MeI is due to the nucleophilicity of the I^- ion generated by the reaction, as reported elsewhere.[24] Besides, methylating agents not only react with the Py group of the ligands, but with the –S moiety of the Au–S bonds as well. Their reaction with the –S group causes the Au–S bond to break, leading to the decomposition of the clusters. Me_3OBF_4 likely decomposed the clusters owing to its strong reactivity. On the other hand, Me_2SO_4 and TfOMe selectively react with the outer Py groups over the inner –S groups because of their moderate reactivity, allowing the methylation reaction to proceed without any decomposition of the clusters.

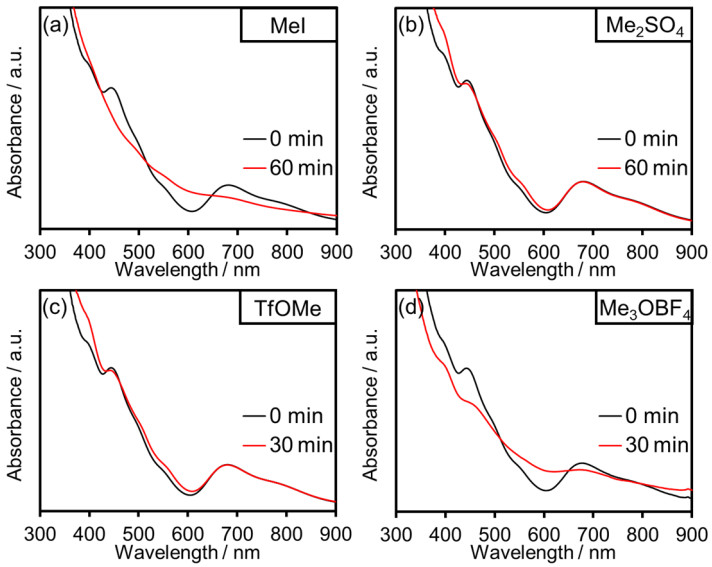

Figure 1. Selection of methylating reagents. UV-vis absorption spectra of the samples before (0 min) and after reaction (30 min or 60 min) with (a) MeI, (b) Me_2SO_4, (c) TfOMe, and (d) Me_3OBF_4.

TfOMe, which proceeded the most efficiently (see ESI-MS results in Figures S2-S4), was selected as the methylating reagent. The Menshutkin reaction on the $Au_{25}(4\text{-PyET})_{18}$ cluster was conducted to obtain methylated, cationized Au_{25} clusters (see the detailed procedure in the Supporting Information). Trifluoromethanesulfonic acid (CF_3SO_2OH) was noted as a decomposition product of TfOMe, which could hinder the Menshutkin reaction by protonating the unreacted Py groups. By performing the 1h reaction 3 times (i.e., 3 cycles), CF_3SO_2OH was effectively removed and the reaction was proceeded efficiently. Notably, running 1 cycle for up to 2 days did not produce fully methylated Au clusters as the main product and was less efficient than the 3-cycle reaction (Figure S5). UV-vis absorption spectra of the sample before and after 1 cycle showed slight increases in the characteristic Au_{25} cluster bands[22,23] at 400 and 560 nm, whereas those at 450, 670, and 780 nm slightly decreased (Figure 2). Such absorption changes were also observed when $Au_{25}(4\text{-PyET})_{18}$ clusters were treated with HCl, in which the reversible protonation of the Py group gave its positive form, $–C_5H_4NH^+$.[21] These results strongly suggest that the geometric structure of Au_{25} core was distorted due to the surface charge anisotropy[12,21] during the addition of positive charges. The absorption spectra showed negligible changes after the 2nd and 3rd reaction cycles (Figure S6), demonstrating the good stability of the methylated, cationized Au_{25} clusters and lack of geometrical changes in the Au_{25} core (discussed in detail in Figure 4).

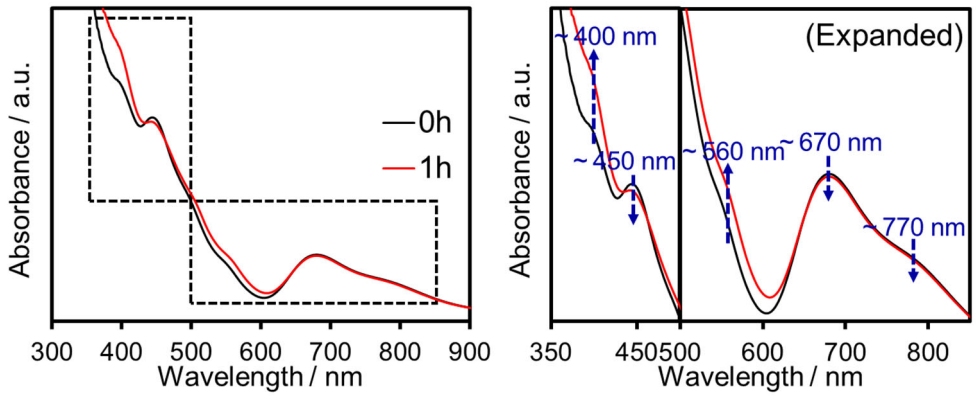

Figure 2. UV-vis absorption spectra of the sample before (0h) and after 1-cycle reaction (1h) with TfOMe.

The positive-mode ESI-MS of the methylated Au_{25} clusters (Figure 3, left) showed 3 different charged states +2, +3, and +4 (depending on the number of attached PF_6^- anions). Specifically, $[Au_{25}^{-1}(4\text{-PyET-}CH_3^+)_x(4\text{-PyET})_{18-x}\cdot(PF_6^-)_{x-3}]^{2+}$ ($11 \le x \le 18$), $[Au_{25}^{-1}(4\text{-PyET-}CH_3^+)_x(4\text{-PyET})_{18-x}\cdot(PF_6^-)_{x-4}]^{3+}$ ($12 \le x \le 18$), and $[Au_{25}^{-1}(4\text{-PyET-}CH_3^+)_x(4\text{-PyET})_{18-x}\cdot(PF_6^-)_{x-5}]^{4+}$ ($14 \le x \le 18$) (groups $Au_{25}(+2)$, $Au_{25}(+3)$, and $Au_{25}(+4)$, respectively) were observed. Figure 3 (right) shows the expanded ESI-MS of the methylated Au_{25} clusters with +3 charged state (group $Au_{25}(+3)$) observed with relatively high intensity (expanded ESI-MS of group $Au_{25}(+2)$ and $Au_{25}(+4)$ in Figure S7). After 1st reaction cycle (1h in total), the *x* values (the number of methylated ligands) ranged between 12 and 18. Note that after 2 min of reaction, *x* had already reached 10-18, indicating the reaction rate became very inefficient due to the decrease in the number of reaction sites and bulkiness of the counter anions $CF_3SO_3^-$ and PF_6^-, which geometrically impede further reaction of the unreacted ligands (Figure S2). After the 2nd and 3rd reaction cycles (2h and 3h in total, respectively), the *x* values increased to *x*=14-18 and 15-18 respectively. The average number of methylated ligands was calculated from the peak intensity ratio, assuming the mass spectral signal intensities are equal to the solution concentrations of the corresponding cluster species; the numbers for cycles 1-3 were 15.0 (83.1%), 16.7 (92.7%), and 17.3 (95.9%), respectively (refer to detailed calculation procedures in Table S1). The ^1H NMR spectrum of the sample after the 3rd reaction cycle (Figure S8) also showed a similar *x* value of 17.3 (96.0%), confirming that the *x* values calculated from the mass spectral signal intensities are reliable in the selected mass region (*m/z* = 2220-4950). The average *x* value gradually increased by the number of reaction cycles, and nearly per-methylated Au_{25} clusters were successfully obtained after 3 cycles. By further increasing the number of reaction cycles to 4 (4h in total), more clusters, with *x*=18, could be produced; however they exhibited more impurity peaks due to their decomposition (Figure S9). The compositions and charge assignments of the observed Au_{25} cluster peaks are summarized in Table 1. The isotope distributions matched well with the simulated isotope patterns (Figure S10). The well-known fragmentation product $[Au_4^0(4\text{-PyET-}CH_3^+)_x(4\text{-PyET})_{4-x}\cdot(PF_6^-)_{x-1}]^{1+}$ ($1 \le x \le 4$) was also observed (Figure S11). Moreover, the fragmentation products during the ESI process $[Au_{24}^0(4\text{-PyET-}CH_3^+)_x(4\text{-PyET})_{16-x}\cdot(PF_6^-)_{x-3}]^{3+}$ ($8 \le x \le 16$) and $[Au_{23}^0(4\text{-PyET-}CH_3^+)_x(4\text{-PyET})_{15-x}\cdot(PF_6^-)_{x-3}]^{3+}$ ($8 \le x \le 15$) were observed for $Au_{25}(SR)_{18}$; these corresponded to losses of $Au_1–SR_2$ and $Au_2–SR_3$ (Figure S11). Interestingly, like those of the whole Au_{25} clusters, the *x* values of these fragmentation products also increased with the number of reaction cycles (see the summary of compositions and charge assignments in Table S2). Note that the

methylated (x = 17.3) sample showed less thermal stability than neutral (x = 0) one in solution owing to its highly charged surface structures (Figure S13).

We also evaluated the weaker methylating reagent, Me_2SO_4, by varying the reaction time and number of reaction cycles; this gave clusters with various x values. Specifically, those with x=8.5, 9.7, 12.6, and 14.1 were formed by reactions with Me_2SO_4 for times of 2, 5, 15, and 60 min, respectively (see Figure S3 and Table S3). The abundance ratios of each cluster species with different x values, determined by the intensities of their ESI-MS peaks, are shown in Figure 4. Monitoring the reaction with Me_2SO_4 revealed that the absorption spectral changes (i.e., the structural change of Au_{25} core) were completed at 15 min, where the minimum x value of the contained Au clusters was 9 (Figure S12). These observations indicate that the structural changes are complete when approximately half number of the surface Py groups are cationized. To further understand the mechanisms of the spectral and structural changes caused by the dense surface charges, we are currently isolating each cluster species and analyzing them by single-crystal X-ray structure analysis.

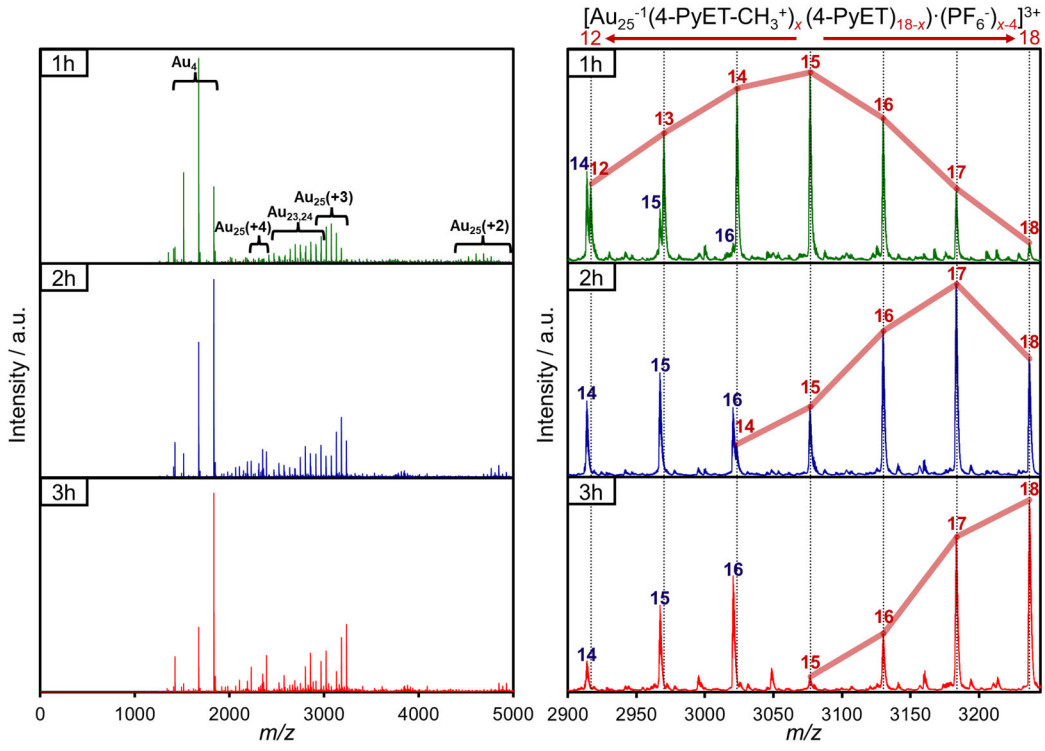

Figure 3. Positive-mode ESI-MS of the samples after different numbers of reaction cycles with TfOMe (left), and the expanded ESI-MS of group Au_{25}(+3) (right). The red and blue numbers indicate the x values of $[Au_{25}^{-1}(4\text{-PyET-CH}_3^+)_x(4\text{-PyET})_{18-x}\cdot(PF_6^-)_{x-4}]^{3+}$ and fragmentation product $[Au_{24}^{0}(4\text{-PyET-CH}_3^+)_x(4\text{-PyET})_{16-x}\cdot(PF_6^-)_{x-3}]^{3+}$, respectively.

Table 1. The compositions and charge assignments of the observed Au_{25} cluster peaks in Figure 3.

x value	Composition	1h *m/z* (obs.)	2h *m/z* (obs.)	3h *m/z* (obs.)	*m/z* (calc.)
Total charge +2 : $Au_{25}^{-1}(4\text{-PyET-CH}_3^+)_x(4\text{-PyET})_{18-x}\cdot(PF_6^-)_{x-3}$					
11	$Au_{25}^{-1}(4\text{-PyET-CH}_3^+)_{11}(4\text{-PyET})_7(PF_6^-)_8$	4368.38	-	-	4368.40
12	$Au_{25}^{-1}(4\text{-PyET-CH}_3^+)_{12}(4\text{-PyET})_6(PF_6^-)_9$	4448.39	-	-	4448.40
13	$Au_{25}^{-1}(4\text{-PyET-CH}_3^+)_{13}(4\text{-PyET})_5(PF_6^-)_{10}$	4528.38	-	-	4528.38
14	$Au_{25}^{-1}(4\text{-PyET-CH}_3^+)_{14}(4\text{-PyET})_4(PF_6^-)_{11}$	4608.36	4608.36	-	4608.38
15	$Au_{25}^{-1}(4\text{-PyET-CH}_3^+)_{15}(4\text{-PyET})_3(PF_6^-)_{12}$	4688.37	4688.38	4688.31	4688.37
16	$Au_{25}^{-1}(4\text{-PyET-CH}_3^+)_{16}(4\text{-PyET})_2(PF_6^-)_{13}$	4768.35	4768.36	4768.37	4768.36
17	$Au_{25}^{-1}(4\text{-PyET-CH}_3^+)_{17}(4\text{-PyET})_1(PF_6^-)_{14}$	4848.33	4848.36	4848.36	4848.36
18	$Au_{25}^{-1}(4\text{-PyET-CH}_3^+)_{18}(PF_6^-)_{15}$	-	4928.34	4928.34	4928.35
Total charge +3 : $Au_{25}^{-1}(4\text{-PyET-CH}_3^+)_x(4\text{-PyET})_{18-x}\cdot(PF_6^-)_{x-4}$					
12	$Au_{25}^{-1}(4\text{-PyET-CH}_3^+)_{12}(4\text{-PyET})_6(PF_6^-)_8$	2917.30	-	-	2917.28
13	$Au_{25}^{-1}(4\text{-PyET-CH}_3^+)_{13}(4\text{-PyET})_5(PF_6^-)_9$	2970.62	-	-	2970.61
14	$Au_{25}^{-1}(4\text{-PyET-CH}_3^+)_{14}(4\text{-PyET})_4(PF_6^-)_{10}$	3023.94	3023.95	-	3023.94
15	$Au_{25}^{-1}(4\text{-PyET-CH}_3^+)_{15}(4\text{-PyET})_3(PF_6^-)_{11}$	3077.27	3077.28	3077.27	3077.27
16	$Au_{25}^{-1}(4\text{-PyET-CH}_3^+)_{16}(4\text{-PyET})_2(PF_6^-)_{12}$	3130.59	3130.60	3130.61	3130.60
17	$Au_{25}^{-1}(4\text{-PyET-CH}_3^+)_{17}(4\text{-PyET})_1(PF_6^-)_{13}$	3183.92	3183.92	3183.93	3183.92
18	$Au_{25}^{-1}(4\text{-PyET-CH}_3^+)_{18}(PF_6^-)_{14}$	3237.24	3237.25	3237.25	3237.25
Total charge +4 : $Au_{25}^{-1}(4\text{-PyET-CH}_3^+)_x(4\text{-PyET})_{18-x}\cdot(PF_6^-)_{x-5}$					
14	$Au_{25}^{-1}(4\text{-PyET-CH}_3^+)_{14}(4\text{-PyET})_4(PF_6^-)_9$	2231.72	-	-	2231.71
15	$Au_{25}^{-1}(4\text{-PyET-CH}_3^+)_{15}(4\text{-PyET})_3(PF_6^-)_{10}$	2271.71	2271.71	2271.71	2271.71
16	$Au_{25}^{-1}(4\text{-PyET-CH}_3^+)_{16}(4\text{-PyET})_2(PF_6^-)_{11}$	2311.70	2311.71	2311.70	2311.70
17	$Au_{25}^{-1}(4\text{-PyET-CH}_3^+)_{17}(4\text{-PyET})_1(PF_6^-)_{12}$	2351.70	2351.70	2351.69	2351.70
18	$Au_{25}^{-1}(4\text{-PyET-CH}_3^+)_{18}(PF_6^-)_{13}$	2391.69	2391.69	2391.69	2391.69

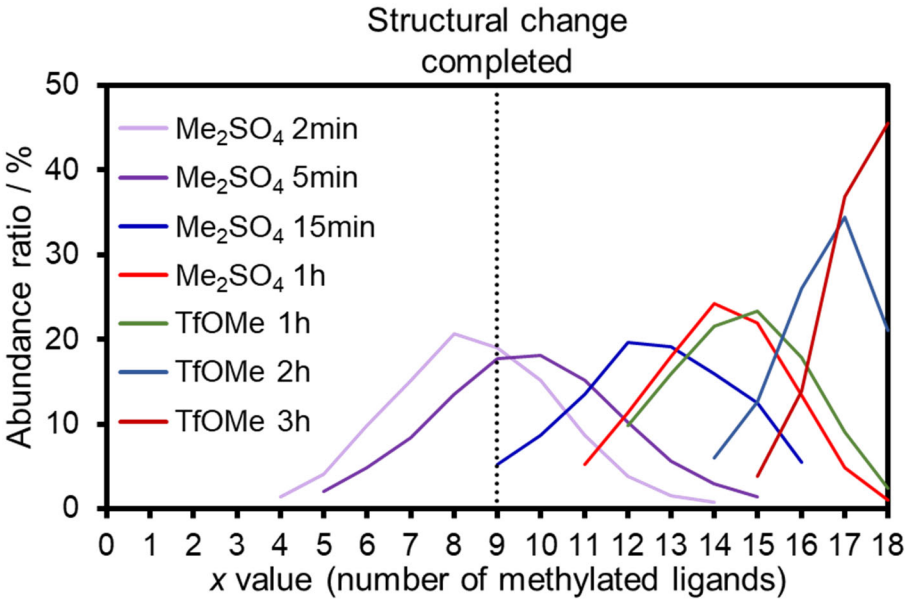

Figure 4. The abundance ratios of each cluster species with different *x* values under representative conditions.

We have demonstrated a novel method for obtaining cationized Au clusters via the surface Menshutkin S_N2 reaction. By changing the methylating reagent, reaction time, and number of reaction cycles, we succeeded in controlling the number of methylated ligands (*x*); an *x* of approximately 18 (i.e., fully methylated Au_{25}(4-PyET-CH_3^+)$_{18}$) was obtained under the optimal condition. This work proposed not only a new synthetic pathway for cationized Au clusters, but also provides a novel idea for diversifying the R-groups of molecular metal clusters through the surface chemical reaction.

Supporting Information

The Supporting Information is available free of charge on the ACS Publications website.

Experimental details and supplementary data (UV-vis absorption spectra, ESI-MS, and ^{1}H-NMR spectrum). (PDF)

Corresponding Author

ishida-yohei@eng.hokudai.ac.jp (Y. I.);

tetsu@eng.hokudai.ac.jp (T. Y.).

Notes

The authors declare no competing financial interest.

ACKNOWLEDGEMENT

Y.I. thanks financial supports from JSPS KAKENHI grant number 21K04805, JKA and its promotion funds from KEIRIN RACE, Ogasawara Toshiaki Memorial Foundation, Tanaka Kikinzoku Memorial Foundation, Iketani Science and Technology Foundation, The Foundation for The Promotion of Ion Engineering, and JFE 21st Century Foundation. Partial financial supports by KAKENHI (21H00138 and 18KK0159 to T.Y.) from JSPS and JKA and its promotion funds from KEIRIN RACE (113) are gratefully acknowledged.

(1) Li, G.; Jin, R. Atomically Precise Gold Nanoclusters as New Model Catalysts. *Acc. Chem. Res.* **2013**, *46*, 1749–1758.

(2) Wan, X. K.; Wang, J. Q.; Nan, Z. A.; Wang, Q. M. Ligand effects in catalysis by atomically precise gold nanoclusters. *Sci. Adv.* **2017**, *3*, No. e1701823.

(3) Guan, G.; Zhang, S. Y.; Cai, Y.; Liu, S.; Bharathi, M. S.; Low, M.; Yu, Y.; Xie, J.; Zheng, Y.; Zhang, Y. W., Han, M. Y. Convenient Purification of Gold Clusters by Co-Precipitation for Improved Sensing of Hydrogen Peroxide, Mercury Ions and Pesticides. *Chem. Commun.* **2014**, *50*, 5703–5705.

(4) Shen, R., Liu, P., Zhang, Y., Yu, Z., Chen, X., Zhou, L., Nie, B; Żaczek, A.; Chen, J; Liu, J. Sensitive Detection of Single-cell Secreted H_2O_2 by Integrating a Microfluidic Droplet Sensor and Au Nanoclusters. *Anal. Chem.* **2018**, *90*, 4478–4484.

(5) Zheng, K.; Setyawati, M. I.; Leong, D. T.; Xie, J. Surface Ligand Chemistry of Gold Nanoclusters Determines Their Antimicrobial Ability. *Chem. Mater.* **2018**, *30*, 2800–2808.

(6) Zheng, K.; Setyawati, M. I.; Leong, D. T.; Xie, J. Antimicrobial Gold Nanoclusters. *ACS Nano*, **2017**, *11*, 6904–6910.

(7) Chen, Y.; Zeng, C.; Kauffman, D. R.; Jin, R. Tuning the Magic Size of Atomically Precise Gold Nanoclusters via Isomeric Methylbenzenethiols. *Nano Lett.* **2015**, *15*, 3603–3609.

(8) Yan, J.; Teo, B. K.; Zheng, N. Surface Chemistry of Atomically Precise Coinage-Metal Nanoclusters: From Structural Control to Surface Reactivity and Catalysis. *Acc. Chem. Res.* **2018**, *51*, 3084–3093.

(9) Ackerson, C. J.; Jadzinsky, P. D.; Kornberg, R. D. Thiolate Ligands for Synthesis of Water-Soluble Gold Clusters. *J. Am. Chem. Soc.* **2005**, *127*, 6550–6551.

(10) Knoppe, S.; Bürgi, T. Chirality in Thiolate-protected Gold Clusters. *Acc. Chem. Res.* **2014**, *47*, 1318–1326.

(11) Yang, H.; Wang, Y.; Lei, J.; Shi, L.; Wu, X.; Makinen, V.; Lin, S.; Tang, Z.; He, J.; Hakkinen, H.; Zheng, L.; Zheng, N. Ligand-Stabilized $Au_{13}Cu_x$ (x = 2, 4, 8) Bimetallic Nanoclusters: Ligand Engineering to Control the Exposure of Metal Sites. *J. Am. Chem. Soc.* **2013**, *135*, 9568–9571.

(12) Yuan, X.; Goswami, N.; Chen, W.; Yao, Q.; Xie, J. Insights into the Effect of Surface Ligands on the Optical Properties of Thiolated Au_{25} Nanoclusters. *Chem. Commun.* **2016**, *52*, 5234–5237.

(13) Nel, A. E.; Mädler, L.; Velegol, D.; Xia, T.; Hoek, E. M.; Somasundaran, P.; Klaessig, F.; Castranova, V.; Thompson, M. Understanding biophysicochemical interactions at the nano-bio interface. *Nat. Mater.* **2009**, *8*, 543−557.

(14) Ishida, Y.; Narita, K.; Yonezawa, T.; Whetten, R. L. Fully Cationized Gold Clusters: Synthesis of $Au_{25}(SR^+)_{18}$. *J. Phys. Chem. Lett.* **2016**, *7*, 3718–3722.

(15) Narita, K; Ishida, Y.; Yonezawa, T; Huang, Z. Super Polycationic Molecular Compounds: $Au_{144}(SR^{+})_{60}$ Clusters. *J. Phys. Chem. C* **2019**, *123*, 21768−21773.
(16) Huang, Z.; Ishida, Y.; Narita, K; Yonezawa, T. Kinetics of Cationic-Ligand-Exchange Reactions in Au_{25} Nanoclusters. *J. Phys. Chem. C* **2018**, *122*, 18142−18150.
(17) Fields-Zinna, C. A.; Sardar, R.; Beasley, C. A.; Murray, R. W. Electrospray Ionization Mass Spectrometry of Intrinsically Cationized Nanoparticles, $[Au_{144/146}(SC_{11}H_{22}N(CH_2CH_3)_3{}^{3+})_X(S(CH_2)_5CH_3)_Y]^{X+}$. *J. Am. Chem. Soc.* **2009**, *131*, 16266−16271.
(18) Gunawardene, P. N.; Corrigan, J. F.; Workentin, M. S. Golden Opportunity: A Clickable Azide-Functionalized $[Au_{25}(SR)_{18}]^{-}$ Nanocluster Platform for Interfacial Surface Modifications, *J. Am. Chem. Soc.* **2019**, *141*, 11781−11785.
(19) Cui, X.; Wang, J.; Liu, B.; Ling, S.; Long, R.; Xiong, Y. Turning Au Nanoclusters Catalytically Active for Visible-Light-Driven CO_2 Reduction through Bridging Ligands, *J. Am. Chem. Soc.* **2018**, *140*, 16514−16520.
(20) Menschutkin, N. Beiträge zur Kenntnis der Affinitätskoeffizienten der Alkylhaloide und der organischen Amine. *Z. Phys. Chem.* **1890**, *5*, 589−600.
(21) Huang, Z.; Ishida, Y.; Yonezawa, T. Basic $[Au_{25}(SCH_2CH_2Py)_{18}]^{-}\cdot Na^{+}$ Clusters: Synthesis, Layered Crystallographic Arrangement, and Unique Surface Protonation. *Angew. Chem., Int. Ed.* **2019**, *58*, 13411–13415.
(22) Negishi, Y.; Chaki, N. K.; Shichibu, Y.; Whetten, R. L.; Tsukuda, T. Origin of Magic Stability of Thiolated Gold Clusters: a Case Study on $Au_{25}(SC_6H_{13})_{18}$. *J. Am. Chem. Soc.* **2007**, *129*, 11322–11323.
(23) Zhu, M.; Aikens, C. M.; Hollander, F. J.; Schatz, G. C.; Jin, R. Correlating the Crystal Structure of a Thiol-Protected Au_{25} Cluster and Optical Properties. *J. Am. Chem. Soc.* **2008**, *130*, 5883–5885.
(24) Zhu, M.; Chan, G.; Qianb, H.; Jin, R. Unexpected Reactivity of $Au_{25}(SCH_2CH_2Ph)_{18}$ Nanoclusters with Salts, *Nanoscale*, **2011**, *3*, 1703–1707.